Properties of the solid-liquid interface layer of growing ice crystals: A dynamic light scattering study

P. Böni,* J. H. Bilgram, and W. Känzig
Laboratorium für Festkörperphysik, Eidgenössische Technische Hochschule Zürich, CH-8093 Zürich, Switzerland
(Received 19 May 1983)

The dynamics of solidification are investigated at the ice-water interface by means of Rayleigh-Brillouin spectroscopy. If a critical growth velocity is exceeded, Rayleigh scattering occurs in a layer which has a thickness between 1.4 and 6 μm and a density between water and ice, close to that of water. At constant intensity the width Γ of the central line is proportional to the square of the scattering vector $\vec{k}$, $\Gamma = D_i k^2$, independent of the orientation of $\vec{k}$ relative to the interface. The measured diffusion constants D_i are in the range $1.4\times10^{-8} < D_i < 5.7\times10^{-8}$ cm^2 s^{-1} and isotropic in space. The intensity of the scattered light depends on the heat flow from the liquid into the solid and on the growth velocity. The linewidth of the scattered light decreases with increasing scattering intensity, and vice versa. We interpret D_i as an effective thermal diffusion constant that describes the transport of heat involving fluctuations of order and disorder in the layer (Frenkel's "structure diffusion"). The increase of the total scattering intensity corresponds to an increase of the isothermal compressibility by a factor of 700 as compared to water.

I. INTRODUCTION

Little is known on the nature of the solid-liquid interface of growing crystals. Most theories are based on the assumption of a sharp interface where the atoms become attached.[1] Because the grain boundary energy is larger than two times the interfacial energy between the solid and its melt (case of copper, silver, and gold) Hilliard and Cahn[2] concluded that the interface is diffuse. They developed a theory of the interfacial free energy (squared gradient theory) of nonuniform systems,[3] which was reformulated by Widom[4] and Fisk and Widom[5] for a fluid near its critical point. Experimental results have been compared with these theories.[6] Landau and Lifshitz[7] predict that no critical point exists for the solid-liquid phase transition because the symmetry of the crystal cannot change continuously. Since they disregarded lattice defects this statement may have to be revised, perhaps using the concept of correlation functions. Recently Voronel *et al.*[8] found a critical point in the vicinity of the liquidus line of of a K-Cs alloy. Saito and Müller-Krumbhaar[9] applied a spin-1 antiferromagnetic Ising model to crystal growth from the gas phase. For a certain range of parameters the phase transition proceeds from the gas to a disordered solid and from there to the ordered solid.

The solid-liquid interface of H_2O (Refs. 10 and 11), salol (salicylic acid phenyl ester, $C_6H_4OHCOOC_6H_5$) (Ref. 12), and D_2O (Ref. 13) has been investigated by means of dynamic light scattering. The following results were obtained: The linewidth of the scattered light is proportional to the square of the scattering vector $\vec{k}$ (measured for $\vec{k}$ parallel to the interface). The linewidth can be tentatively interpreted assuming a fluctuating sharp interface.[10,12] Light scattering is only observed once a minimum growth velocity has been exceeded.

In the present work, light scattering experiments are described where the scattering vector is no longer parallel to the interface. The onset of scattering and its hysteretic behavior is investigated for different temperature distributions at the interface. The relation between scattered intensity and linewidth is compared with analogous results observed at critical phenomena.

II. EXPERIMENTAL

A. Experimental setup

We have investigated Rayleigh and Brillouin scattering at the solid-liquid interface of an ice crystal growing into a molten zone. The experimental setup is similar to the one used in earlier work.[10] The zone-melting apparatus (Fig. 1) and the photodetection unit are placed in a cold room at $-18°$. The laser (Spectra Physics 165 argon ion) and the data processing units are placed outside. The laser beam passes through Brewster windows into the cold room. By means of the mirrors $M1$ and $M2$ and the lens L ($f = 500$ mm) the beam can be focused on the interface in a range of angles of incidence ψ_0 between 55° and 90° (Fig. 2). The scattered light is either directly detected with a photomultiplier or analyzed by means of a Fabry-Pérot interferometer for different directions of observation defined by the azimuthal angle Θ and the polar angle ψ. Details concerning the preparation of the crystals and the interface are described in a previous paper.[10]

The growth rate of the crystal is determined by the temperatures of the heating and cooling bath. The position of the interface relative to the laboratory system is held fixed by means of a feedback and control system. A He-Ne laser beam (5 mW) passes in almost grazing incidence over the interface. The intensity of the direct beam is monitored by means of a photoresistor. When the interface rises above the desired level part of the beam is reflected

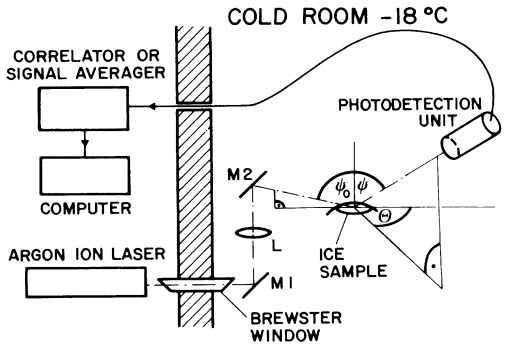

FIG. 1. Experimental setup.

at the vertically curved part of the interface and the intensity of the direct beam is reduced. The signal is processed by a regulator that controls the lowering of the growth tube into the cooling bath by maintaining the detected intensity constant.

B. Dynamic light scattering

The detection system (Fig. 3) for Rayleigh scattering is almost the same as described by Haller.[14] The basal plane of the crystal is imaged by the lens $L1$ ($f=50$ mm) on the aperture $A1$ (vertical slit, 0.1×2 mm^2) that determines the scattering volume. For its inspection during photon counting half of the scattered light is directed by a beam splitter $M1$ to a video camera. Light scattered by dust is

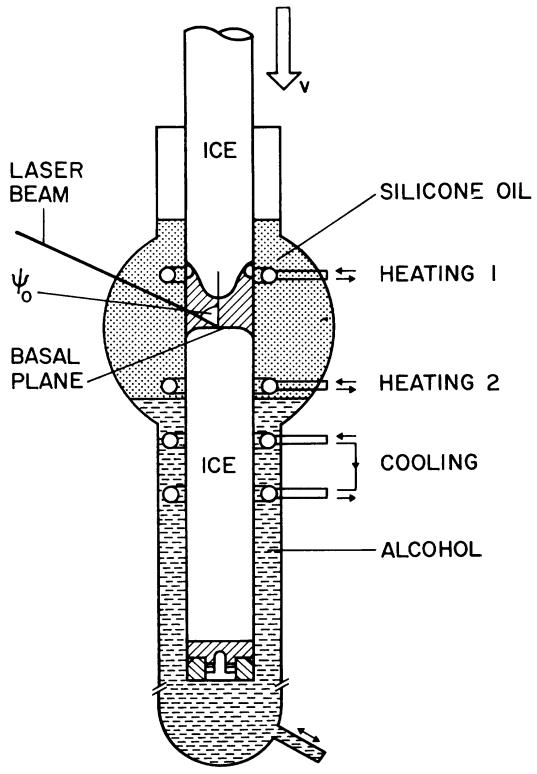

FIG. 2. Zone melting apparatus.

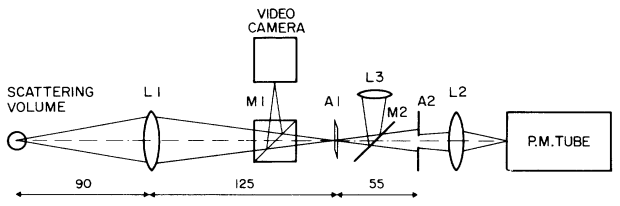

FIG. 3. Optics in front of the photomultiplier (dimensions in mm). L, lenses; M, mirrors; A, apertures.

easily recognized on a television monitor. The effective scattering volume is selected visually using the mirror $M2$ and an eyepiece. The aperture $A2$ (diameter of 0.25 mm) serves to limit the uncertainty of the scattering angle. The lens $L2$ ($f=30$ mm) collects the light and guides it to the cathode of the photomultiplier tube (EMI 9813KB). The discriminator-preamplifier is described in Ref. 15. The photon counts are autocorrelated by a 128-channel multibit (multiple binary digit) correlator (Malvern 7025) interfaced to a minicomputer (Minc 11, of Digital Equipment Corporation).

C. Brillouin scatttering

Brillouin spectra of the interface region are obtained using the simple optical system depicted in Fig. 4. The light scattered parallel to the basal plane at $\Theta=90°$ is collected by the lens $L1$ ($f=150$ mm) and analyzed by a piezoelectrically scanned Fabry-Pérot interferometer (Burleigh RC-10) located in a box, where the temperature is kept constant within 0.02 °C. The piezoelectric stacks are driven by a modified commercial ramp generator (Burleigh RC-42) at one sweep per second. The free spectral ranges are 7.30 GHz for the measurement of the Brillouin lines emerging from the water side of the basal plane and 5.56 GHz for the ice side. The diaphragm $A1$ (diameter of 2 mm) reduces the active area of the mirrors (98.5% reflectivity at 488 nm) and thereby the influence of surface imperfections on them. The lens $L2$ ($f=254$ mm) together with the pinhole $A2$ (diameter of 0.25 mm) serve for spatial filtering. The light is detected by a photomultiplier tube (EMI 9813KB) connected to the Malvern correlator in the signal averaging mode which is triggered by the ramp generator. In order to eliminate the contribution of Raman scattering a 488-nm interference filter F is placed in front of the photomultiplier. The mirror M and

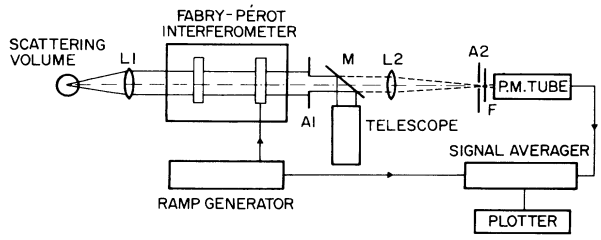

FIG. 4. Fabry-Pérot interferometer facility. L, lenses; M, mirror; A, apertures; F 488-nm filter.

the telescope serve for the selection of the scattering volume and for alignment procedures. The refinement of the spectrometer is about 35.

D. Temperature measurements at the basal plane

The temperature distribution near the basal plane determines the growth velocity of the ice crystal and with it also the onset of light scattering. A simple method to measure the temperature gradient in the ice below the basal plane is the freezing of a thermocouple into the crystal at approximately constant growth velocity. Since light scattering is strongly influenced by crystal defects and dust it is not possible to measure light scattering and temperature gradient in one and the same experiment. However, one can easily reproduce the growth conditions for a crystal (not used during light scattering) with an inserted thermocouple.

Seven different standard temperature distributions were used, each determined by the choice of the temperature of the cooling bath (between $-78\,^{\circ}C$ and $-10\,^{\circ}C$) and of the temperature of the heating bath (between $3\,^{\circ}C$ and $10\,^{\circ}C$). The copper Constantan wires (diameter of 0.07 mm) forming the thermocouple lead from the top of the zone refining tube along the wall. At half height there is a 90° bend so that the measuring junction is at the tube axis. This arrangement minimizes the influence of the thermocouple on the temperature distribution near the basal plane. The reference junction is in an ice-water bath and the voltage is recorded by means of a stripchart recorder. The accuracy of the measured temperatures is $\pm 0.01\,^{\circ}C$.

Overnight a zone is molten below the thermocouple. Then temperature and growth velocity v are recorded during a run for one of the standard temperature distributions. The simultaneous measurement of the temperatures close to the moving solid-liquid interface and of the growth velocity permits the determination of the temperature gradient in the crystal. As a rule it is impossible to measure the gradient above the interface because of convection in the water.

III. EXPERIMENTAL RESULTS

A. Rayleigh scattering

1. *Dependence of the scattered intensity on the angle of incidence*

The intensity of the scattered light is measured after the onset of enhanced Rayleigh scattering (Sec. III D) for different orientations of the scattering vector k relative to the interface by varying the angle of incidence ψ_0 of the laser beam at fixed azimuthal angle Θ. A typical result is shown in Fig. 5 for $\Theta = 140°$. The background arising mainly from Brillouin scattering in the water above the interface is subtracted. The optical axis of the photomultiplier assembly is tilted by 3°—5° ($87° > \psi > 85°$) with respect to the basal plane.

The intensity increases by a factor of about 4 when ψ_0 approaches the angle of total reflection ψ^* ($=79°$). In the range $\psi^* < \psi_0 < 90°$ the intensity has always a second maximum that varies strongly from experiment to experiment between $I(\psi_0) = I(\psi^*)$ and $I(\psi_0) = 2I(\psi^*)$. Similar intensity measurements have been performed at $\Theta = 30°$ and 90°. The results show that the shape of the intensity distribution does not vary with the azimuthal angle Θ. These experiments confirm the earlier conclusion[10] that the light scattering is not due to ice particles suspended in front of the interface. For such a model one would expect a small ψ_0 dependence of the scattered intensity for $\psi_0 < \psi^*$, followed by an increase by a factor of 2, when ψ_0 exceeds ψ^*, due to the fact that the incident as well as the totally reflected beam pass through the scattering layer.

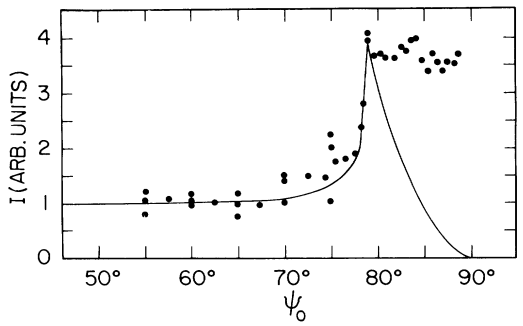

FIG. 5. Dependence of the total scattered intensity on the angle of incidence (growth rate, 1.3 μm/s). Solid line is the calculation for a rough interface.

2. *Linewidth measurements*

The following observations have been made.

(1) The linewidth of the scattered light is independent of the orientation of the scattering vector relative to the basal plane if its length is kept fixed. The variation of the angle of incidence ψ_0 at fixed direction of observation ($\Theta = 90°, \psi = 90°$) parallel to the interface leaves the scattering angle fixed at 90°. Therefore, the length of k is independent of ψ_0, but its orientation changes. Figure 6 shows that the linewidth does not depend upon ψ_0. To measure Γ for $\psi_0 = 0°$ a prism was fused on top of the upper crystal in the zone refining tube in order to reflect the laser beam down the tube axis onto the interface under investigation. For the inverse light path ($\psi_0 = 90°$ and $\psi = 0°$) one measures the same linewidth.

(2) The linewidth is proportional to the square of the scattering vector when k is parallel to the basal plane for scattering angles in the range $5° < \theta < 140°$ corresponding to fluctuation wavelengths in the range $0.19 < \Lambda < 4.2$ μm. Figure 7 shows the result for a growth rate of 1.35 μm/s. The solid circles correspond to scattering angles above 25° and have been measured one after the other; the open circles represent measurements taken at a later time. The scatter of the data becomes larger for reasons to be pointed out later (Sec. III D).

(3) The linewidth is proportional to the square of the scattering vector when k is nearly normal to the basal plane (angle of inclination 9.5°—15°) for scattering angles in the accessible range $15° < \theta < 30°$.

The data points are indicated by triangles in Fig. 7. To minimize stray light from the beam reflected at the inter-

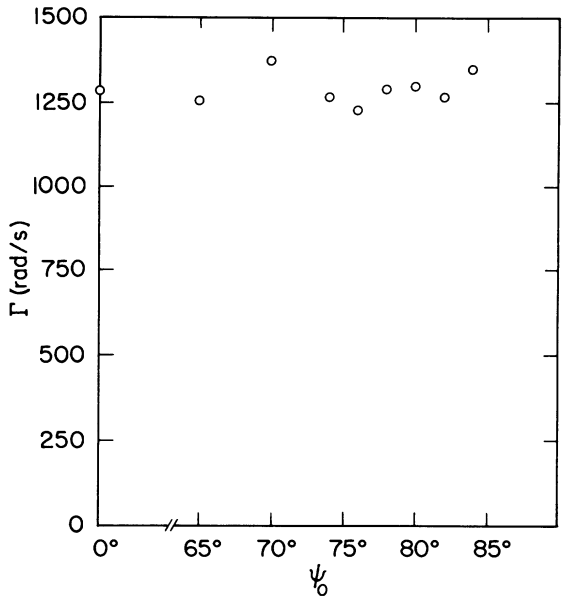

FIG. 6. Dependence of the linewidth on the angle of incidence (growth rate, 1.55 μm/s).

face the basal plane was illuminated from the ice side for angles of incidence $100° < \psi_0 < 115°$, and the scattered light was detected in the direction $\Theta = 0°$ and $\psi = 90°$. The scattering angle is the angle between the wave vector of the refracted light in the water and the wave vector of the scattered light.

(4) The light is scattered at the water side of the interface. The interface is illuminated from the ice side using the same scattering geometry as in (3). If we assume that the light wave is scattered in the ice, the scattering vector $\vec{k}_{ice}$ is defined by

$$\vec{k}_{ice} = \vec{k}_{inc} - \vec{k}_{scatt} , \tag{3.1}$$

where $\vec{k}_{inc}$ is $\vec{k}$ incident in the ice and $\vec{k}_{scatt}$ is $\vec{k}$ scattered parallel to the interface. In this case the linewidth is not proportional to k^2_{ice}. On the other hand, with the assumption that the light wave is first refracted at the solid-liquid interface and then scattered in the melt the scattering vector differs from (3.1):

$$\vec{k}_{water} = \vec{k}_{refract} - \vec{k}_{scatt} , \tag{3.2}$$

where $\vec{k}_{refract}$ is $\vec{k}$ refracted in the water. With this scattering vector the measurements lead to the same proportionality between Γ and k^2 which is observed if the interface is illuminated from the liquid side. As there is no reason to assume that the measured dynamics at the interface depend on the scattering geometry it is concluded that the light is scattered at the water side of the interface.

(5) The linewidths measured simultaneously for two different orientations of the scattering vectors vary in the same way in time. The basal plane was illuminated from the ice side under a fixed angle of incidence $\psi_0 = 103°$. The light was detected nearly parallel to the interface ($\psi = 88°$) alternating between the directions $\Theta = 0°$ and 13° corresponding to scattering angles θ of 17.5° and 20°, respectively. The angles between k and the normal to the interface were 9° and 45°. The normalized linewidths

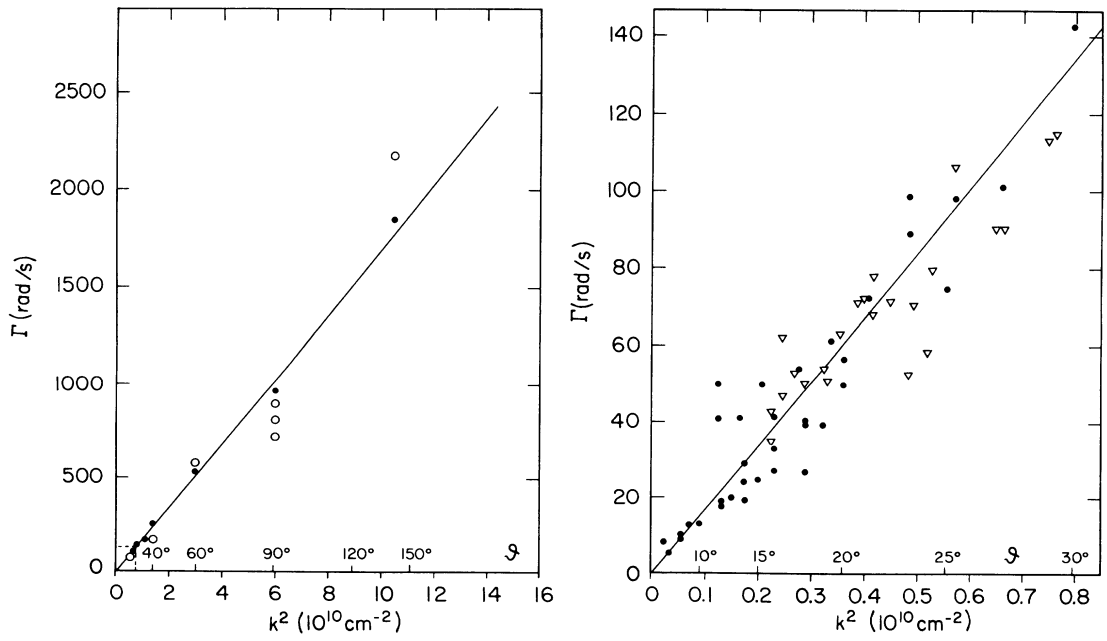

FIG. 7. Linewidths of the light scattered with k parallel (open circles and solid circles) and k perpendicular (triangles) to the solid-liquid interface. Inset is expanded by a factor of 20 (growth rate, 1.35 μm/s).

$$\Gamma_0 = \frac{\Gamma}{\sin^2(\theta/2)} \tag{3.3}$$

are plotted versus time in Fig. 8. They vary the same way in time indicating that their changes originate in changes of the scattering medium and not in the statistics of the autocorrelation function. Within experimental error Γ is proportional to the square of the scattering vector.

(6) The proportionality between Γ and k^2 is independent of the wavelength of light. The linewidth measurements were performed by means of a dye laser (Spectra Physics 375, Rhodamine 6G) in the range of wavelength of light $488 < \lambda < 600$ nm.

B. Brillouin spectra

1. *Brillouin scattering on the liquid side of the phase boundary*

The series of Brillouin spectra reproduced in Fig. 9 were obtained by illuminating the interface from the water side in grazing incidence during the onset of enhanced light scattering ($\Theta = 90°, \psi = 90°$). The measurements demonstrate that the enhanced light scattering at the interface is due to a strong increase of the intensity of the central line and that the intensities of the Brillouin lines do not change. The frequency shift of the Brillouin lines of 5.10 GHz ±0.6% (=0.699 times the free spectral range of the interferometer) agrees with the value given by Teixeira and Leblond[16] for bulk water at 0 °C. The width of the Brillouin lines is 550 MHz ±10%, which is again within the values given by Teixeira and Leblond.

These results are not surprising since the diameter (100 μm) of the laser beam at the interface is more than 16 times the thickness of the interface layer [upper limit, 6 μm (Ref. 10)], so that the volume giving rise to scattering contains only a very small fraction of "anomalous" water.

2. *Brillouin scattering in the solid*

The longitudinal Brillouin components of ice are easy to measure with our Fabry-Pérot interferometer having a free spectral range of 5.56 GHz. The Brillouin frequency of ice at −3 °C is 13.9 GHz.[17] Therefore, the Stokes and anti-Stokes lines overlap in the second and half order of the Brillouin spectrum (2.5×5.56 GHz = 13.9 GHz).

Two types of experiments were performed, both with light incident from the water side. In the first type the angle of incidence ψ_0 is smaller than the angle of total reflection ψ^*, so that light is refracted into the ice. The scattered light is detected from the ice side. The central line is intense because of the contribution from the enhanced Rayleigh scattering at the interface layer. The refracted beam is the primary beam for Brillouin scattering in the ice. The weak line appearing at 2.78 GHz in Fig. 10 is due to the longitudinal mode. The weak lines due to transverse modes (frequency shifts between 6.5 and 7.0 GHz according to Gammon) and the Brillouin lines of water at 5.10 GHz are buried in the strong central line.

In the second type of experiment the incident laser beam is totally reflected at the interface, and the scatter-

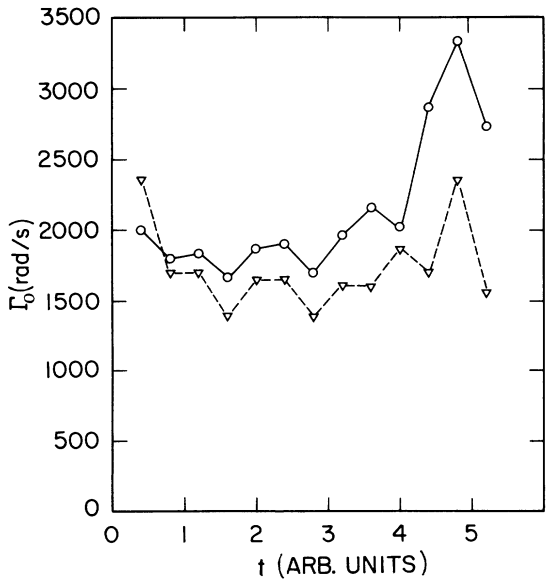

FIG. 8. Normalized linewidths vs time measured simultaneously for two different orientations of the scattering vector relative to the interface (growth rate, 1.35 μm/s at $t=0$ and 0.3 μm/s at $t=5$).

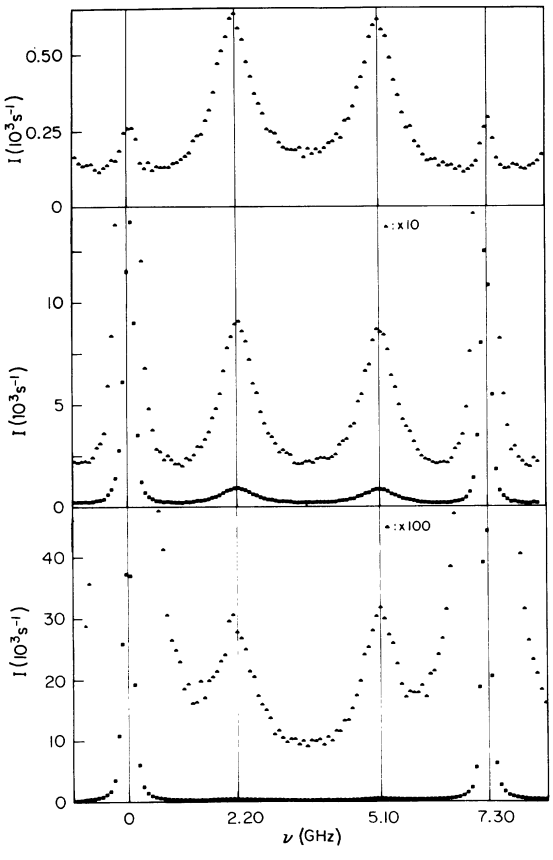

FIG. 9. Series of Brillouin spectra measured at the water side of the interface during the onset of scattering. Magnification of the intensities (triangles) from the top to the bottom is 1, 10, and 100 (scattering angle, 90°). Intensities of the Brillouin lines at 2.2 and 5.1 GHz remain constant whereas the intensity of the central line at 0 GHz increases.

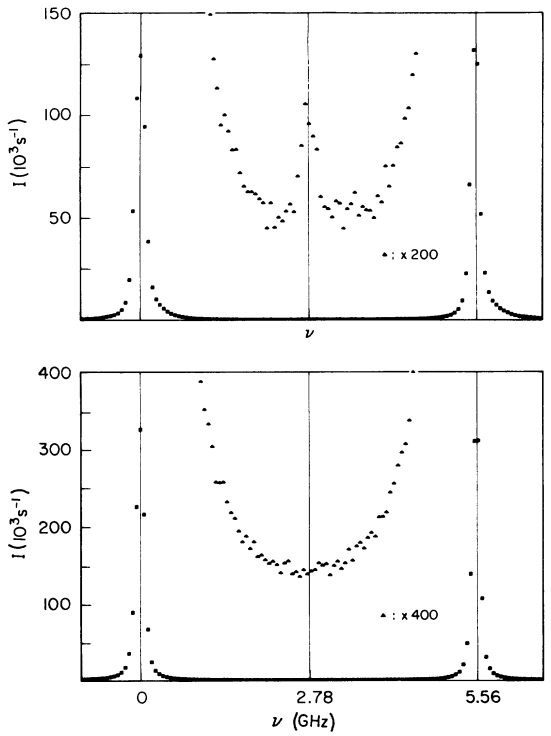

FIG. 10. Brillouin spectra measured at the ice side (top) and at the water side (bottom) of the interface. For details of the scattering geometry see text. Two and one half overlapping orders are shown with two central lines. Shift of the Brillouin line at 2.78 GHz corresponds therefore to a Brillouin frequency of 13.9 GHz.

ing is observed from the water side. Between the two strong peaks due to Rayleigh scattering no resolved Brillouin line can be observed, especially no longitudinal component of ice. No traces of icelike behavior have been detected in the interface region. This result agrees with observation (4) in Sec. III A 2 that the light is scattered at the water side of the interface.

C. Critical-growth-velocity measurements

Güttinger *et al.*[10] have measured the intensity of the light scattered at the ice-water interface versus growth rate. They found that light scattering was observed only if a critical growth velocity $v_c = 1.5$ μm/s was exceeded. We investigated the dependence of the critical growth velocity v_c upon the temperature distribution across the interface.

In Fig. 11 the critical growth velocity v_c is plotted versus the temperature gradient in the ice, G_i, near the interface. The velocity v_c is proportional to G_i within the range $2 < G_i < 4.5$ K/cm. The proportionality is 6.0×10^{-5} cm^2/s K. The measured critical growth velocities for large G_i outside the above limit are smaller than those expected on the basis of linear extrapolation. It is possible that the crystal was growing in region B (see below) during the acceleration of the crystal growth and that light scattering was initiated already at a lower growth velocity.

If the temperature gradient G_w in the water above the interface were zero, the growth velocity of the ice crystal would be determined by Fick's first law,

$$v = \frac{k_i}{L} G_i \ , \tag{3.4}$$

where L is the latent heat and k_i is the thermal conductivity of ice. This function is represented in Fig. 11 by the dashed line. It subdivides into regions A and B. The growth conditions of region A correspond to a negative temperature gradient in the melt. They are not attainable by zone melting and may lead to a Mullins-Sekerka instability.[18] In region B the onset of light scattering is always observed. The interface is stabilized by the positive temperature gradient in the melt, G_w. There is always a heat flow from the melt through the interface to the ice. In region C the interface is also stable and light scattering is observed provided the crystal has been growing under region B conditions. The enhanced Rayleigh scattering disappears once melting of the surface of the crystal has occurred. To produce a new onset of light scattering it is necessary to reach region B. This hysteretic behavior was found for all crystals.

Since region A cannot be investigated during zone melting, it is not known whether dynamic light scattering occurs at an unstable interface. It is expected that the light scattered statically by the inhomogeneities arising from the interface breakdown is very strong and swamps possible dynamic scattering.

D. Onset of scattering

At low growth rates the main contribution to light scattering is Brillouin scattering in the water above the interface. If the growth velocity of the ice crystal exceeds a

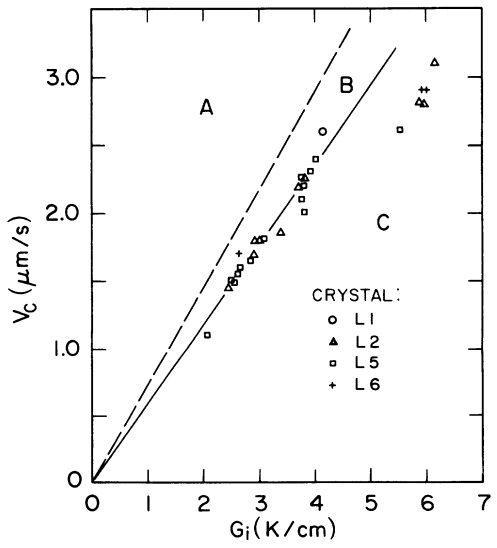

FIG. 11. Critical growth velocity vs temperature gradient in the ice, just beneath the interface. Dashed line separates growth conditions where heat is flowing from the interface into the melt (A) and from the melt to the interface (B and C).

critical value v_c the onset of strong Rayleigh scattering is observed.

The measured intensity autocorrelation function can be fitted by a single exponential

$$G^{(2)}(\tau)\equiv\langle I(t)I(t+\tau)\rangle=A+Be^{-2\tau/C}. \tag{3.5}$$

The value of A is composed of the base value (base line) of the autocorrelation function and of several other contributions, among them Raman and Brillouin scattering. In agreement with the results obtained by Brillouin spectroscopy the measured ratio A/B shows that the Brillouin intensity $2I_B$ is not affected by the onset of Rayleigh scattering.

The growth velocity of the crystal, the intensity of the central line, I_C (dynamical part), and the linewidth of the scattered light have been measured simultaneously. A typical result is plotted in Fig. 12 versus time (crystal $L2$). The interface was illuminated in grazing incidence and the light was detected parallel to the interface under an azimuthal angle $\Theta=90°$. At a growth velocity of 1.45 μm/s enhanced Rayleigh scattering has been visually observed to set in. Arbitrarily we define this time point at $t=0$ s (Fig. 12). At $t=8000$ s the intensity has increased by a factor of about 40 and the linewidth has decreased by about 60%. After 8000 s both quantities would become stationary. Figure 12 does not show this because at $t=8000$ s the temperatures in the zone melting apparatus were readjusted. Although the growth velocity increases during this time interval by only 13% the heat flow through the interface is reduced by $\simeq$25%, as shown by measurements of the temperature gradients. It is not possible to keep growth velocity and heat flow exactly constant during the onset of scattering. The changes of the intensity with time as well as its maximum value differ from experiment to experiment and from crystal to crystal. At $t=8000$ s the growth rate decreases due to the readjusted temperatures in the zone melting apparatus and the intensity decreases. Later the linewidth increases again (outside the range of Fig. 12) with decreasing intensity.

The log-log plot (Fig. 13) of the linewidth versus the intensity I_C demonstrates that the dependence of Γ on I_C (in counts/s) follows a power law

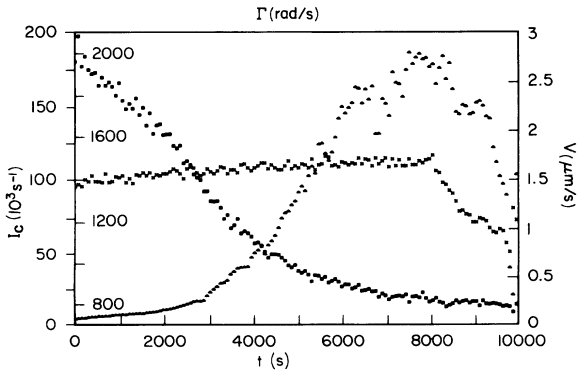

FIG. 12. Time dependence of intensity (triangles), linewidth (squares), and growth velocity (crosses) during the onset of scattering.

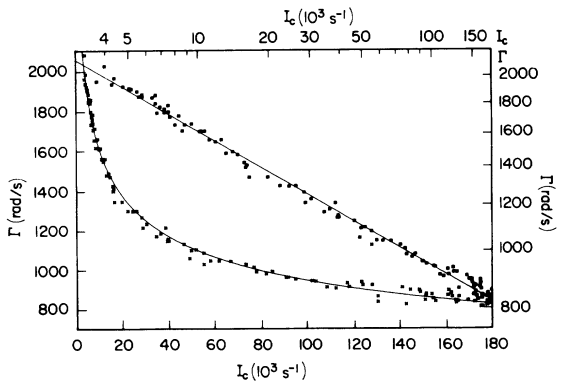

FIG. 13. Linewidth of the scattered light vs the intensity in a linear plot (crosses) and in a log-log plot (squares). Solid lines are obtained by linear regression.

$$\Gamma=f\left[\frac{I_C}{1000\text{ counts/s}}\right]^{-\alpha}, \tag{3.6}$$

where $\alpha=0.23\pm1\%$ and $f=2750$ rad/s $\pm1\%$. The exponents α and parameters f for crystal $L2$ measured at different values of the temperature gradients G_i in the ice using the above scattering geometry are plotted in Fig. 14. Regarding the difficulty of the experiments the reproducibility of the numbers is surprising. The parameters f measured at large G_i are significantly larger than those at smaller G_i indicating that the lifetime of the fluctuations is shorter at high gradients.

E. Influence of crystal quality on light scattering parameters

A necessary condition to obtain reproducible light scattering data is the absence of dust. Dust-free crystals are produced by zone melting. Some qualitative results

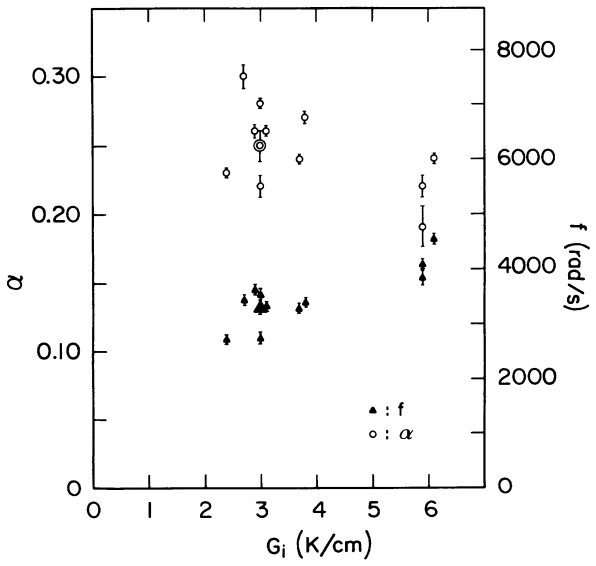

FIG. 14. Dependence of the parameters α (circles) and f (triangles) from Eq. (3.6) on the temperature gradient in the ice. Emphasized points represent data measured during a run where the intensity was decreasing and the linewidth increasing.

TABLE I. Dependence of light scattering parameters on crystal quality. $2I_B$, intensity of the Brillouin lines; I_C, intensity of the central line; G_i, temperature gradient in the ice; α, f, parameters in Eq. (3.6) (mean values).

Grade	$I_C/2I_B$ $G_i<4$ K/cm	$I_C/2I_B$ $G_i\simeq 6$ K/cm	Γ (10^3 rad/s) $G_i<4$ K/cm	Γ (10^3 rad/s) $G_i\simeq 6$ K/cm	α	f (rad/s)
A	4–50	10–60	$0.8<\Gamma<2.4$	$1.2<\Gamma<3.4$	0.25±12%	3450±20%
B	1–10		$1.1<\Gamma<1.7$		0.08±100%	1900±15%
C	0.2–1	not measured	$\simeq 2.7$	not measured	cannot be fitted	

obtained from experiments performed with crystals of three different qualities A, B, and C are summarized in Table I. Crystals without small-angle grain boundary grooves as can be grown from a fresh seed are called grade A, crystals with such grooves near the circumference of the growth tube only are called grade B, and crystals with grooves over the whole interface are called grade C. The crystal quality was judged visually. A more exact characterization (e.g., dislocation density) by x-ray topography cannot be performed without destroying the crystal.

For grade A crystals the maximum intensity I_C is larger and the minimum linewidth is smaller than for crystals of grades B or C ($G_i<4$ K/cm). At high-temperature gradients ($G_i\simeq 6$ K/cm) the intensity range is the same for crystals A and B (C has not been investigated). For crystals of grade A the dependence of the linewidth on the intensity is well described by the power law (3.6) with a mean value $\alpha=0.25\pm 12\%$. For crystals of grade C the dependence of the linewidth on the intensity could not be fitted.

From the above observations we conclude that crystal quality significantly influences linewidth and intensity of the scattered light. It is only for crystals of grade A that it makes sense to give values of α and f. With increasing crystal perfection the exponent α tends to increase. The value $\alpha=0.25$ is rather a lower limit.

F. Dependence of the scattered intensity on the growth conditions

The growth velocity of the ice crystals is controlled by the temperature distribution in the zone melting apparatus. Experiments have been performed at various temperature distributions. By properly adjusting the temperatures the intensity can even increase at decreasing growth velocity. The present experiments indicate that a decreasing heat flow from the water to the ice usually leads to an increase of the intensity of the scattered light. A larger heat flow stabilizes the interface: The critical growth velocity is high, the scattered intensity is small and no Mullins-Sekerka instability is possible.

IV. INTERPRETATION

In this section the intensity and linewidth measurements are interpreted in terms of a layer at the ice-water interface. The model of the rough interface developed in Ref. 10 is ruled out. Then light scattering data measured during the onset of scattering are compared with those arising from critical phenomena.

A. Light scattering from interface fluctuations

The intensity of the light scattered by a rough surface was calculated to first order in the surface roughness by several authors.[19–22] The results were applied by Loudon and Sandercock[23] in an analysis of the light scattering cross section for surface ripples on solids.

We consider an incident beam of cross-sectional area F giving an illuminated surface spot of area $F/\cos\psi_0$ supposed to lie inside the field of view of the detector. According to Loudon and Sandercock[23] the differential scattering cross section is given by

$$\frac{d\sigma}{d\Omega}=\frac{k_i^2 AF\cos^2\psi}{4\pi^2\cos\psi_0}\frac{|A_s|^2}{|A_i|^2}\ . \tag{4.1}$$

The angles ψ_0 and ψ are defined in Fig. 1, k_i is the wave vector of the light, and A is the total surface area. $|A_s|$ and $|A_i|$ are the field amplitudes of the scattered and the incident light. For polarization of the incident light parallel to the plane of incidence the polarization component of the scattered light[20] perpendicular to the plane containing the wave vector of the scattered light and the normal to the interface is

$$A_s^s=2ik_i\zeta_p|A_i|\frac{\tan(\psi_0-\psi_0')\sin\psi}{\sin(\psi+\psi')\tan\psi_0}\sin\Theta\cos\psi_0' \tag{4.2}$$

and for the polarization component parallel to that plane one has

$$A_s^p=-2ik_i\zeta_p|A_i|\frac{\tan(\psi_0-\psi_0')\sin\psi}{\sin(\psi+\psi')\tan\psi_0}\times\frac{\sin\psi\sin\psi_0-\cos\psi'\cos\psi_0'\cos\Theta}{\cos(\psi-\psi')}\ . \tag{4.3}$$

ζ_p is the amplitude of the Fourier component of the surface fluctuation with wave vector p. The angles of refraction ψ_0' and ψ' are given by Snell's law.

The above formulas are used to calculate the intensity of the light scattered by the ice-water interface which is assumed to be rough with amplitudes ζ_p small compared to the wavelength of light. By Snell's law

$$n_w\sin\psi_0=n_i\sin\psi_0'\ . \tag{4.4}$$

$$n_w\sin\psi=n_i\sin\psi'\ , \tag{4.5}$$

the angles of refraction can be calculated. n_w and n_i are the indices of refraction of water and ice. The detection system used in our experiments selected only part of the illuminated surface spot. The area of the observed surface spot is then not $F/\cos\psi_0$ but $b/\cos\psi$, and the result (4.1) has to be multiplied by

$$\frac{\cos\psi_0}{F}\frac{b}{\cos\psi}, \tag{4.6}$$

where b is the cross-sectional area of the detected scattered beam. Inserting (4.2)—(4.6) in (4.1) yields for $\psi > \psi^*$ and $\psi_0 < \psi^*$ and with $n = n_w/n_i$

$$\frac{d\sigma_1}{d\Omega} = \frac{Ab}{\pi^2} k_i^4 |\zeta_p|^2 \cos\psi \frac{\tan^2(\psi_0-\psi_0')}{(\tan^2\psi_0)(n^2-1)} \left[\cos^2\psi_0'\sin^2\Theta + \frac{\sin^2\psi\sin^2\psi_0 + (n^2\sin^2\psi-1)\cos^2\psi_0'\cos^2\Theta}{n^2\sin^2\psi-\cos^2\psi}\right] \tag{4.7}$$

and for $\psi > \psi^*$ and $\psi_0 > \psi^*$

$$\frac{d\sigma_2}{d\Omega} = \frac{Ab}{\pi^2} k_i^4 |\zeta_p|^2 \frac{\cos\psi}{n^2\tan^2\psi_0-1} \left[(n^2\sin^2\psi_0-1)\sin^2\Theta + \frac{[\sin\psi\sin\psi_0-(n^2\sin^2\psi-1)^{1/2}(n^2\sin^2\psi_0-1)^{1/2}\cos\Theta]^2}{n^2\sin^2\psi-\cos^2\psi}\right]. \tag{4.8}$$

Upon variation of Θ from 0° to ±180° expression (4.8) varies only within ±4% and it can be approximated by

$$\frac{d\sigma_2}{d\Omega} \simeq \frac{Ab}{\pi^2} k_i^4 |\zeta_p|^2 \cos\psi \frac{\sin^2\psi\sin^2\psi_0}{(n^2\tan^2\psi_0-1)(n^2\sin^2\psi-\cos^2\psi)}. \tag{4.9}$$

Since the angle of total reflection, $\psi^* = 79.0°$, is rather close to 90°, Eq. (4.9) describes the intensity distribution for scattering vectors nearly parallel to the interface ($\psi^* < \psi, \psi_0 < 90°$). No dependence of the intensity of the scattered light on Θ was observed in this case.[10] Hence the amplitude $|\zeta_p|$ is independent of the wave vector p of the interface fluctuation within the measured range. In most of our experiments the angles ψ and Θ were chosen close to 90° and ψ_0 was varied. In this case Eqs. (4.7) and (4.8) simplify to

$$\frac{d\sigma}{d\Omega} = \begin{cases} \dfrac{Ab}{\pi^2} k_i^4 |\zeta|^2 \cos\psi \dfrac{\tan^2(\psi_0-\psi_0')\cos^2\psi_0}{n^2-1}\left[\dfrac{\cos^2\psi_0'}{\sin^2\psi_0}+\dfrac{1}{n^2}\right], & 0° \le \psi_0 \le \psi^* \\ \dfrac{Ab}{\pi^2} k_i^4 |\zeta|^2 \cos\psi \dfrac{(\sin^2\psi_0)(n^2+n^{-2})-1}{n^2\tan^2\psi_0-1}, & \psi^* \le \psi_0 \le 90°. \end{cases} \tag{4.10}$$

The differential cross section (4.10) is plotted in Fig. 15. At the angle of total reflection there is a maximum which is $(n+1)^2/n^4$ (=3.78) times that for small angles. In the same figure we have plotted the square of the amplitude of the refracted beam at the ice side as calculated by means of the Fresnel formulas[24]

$$|t|^2 = \begin{cases} \left[\dfrac{2n_i n_w\cos\psi_0}{n_i^2\cos\psi_0 + n_w(n_i^2-n_w^2\sin^2\psi_0)^{1/2}}\right]^2, & \psi_0 \le \psi^* \\ \dfrac{4n_i^2 n_w^2\cos^2\psi_0}{n_i^4\cos^2\psi_0 + n_w^4\sin^2\psi_0 - n_i^2 n_w^2}, & \psi_0 \ge \psi^*. \end{cases} \tag{4.11}$$

The correspondence is striking. The maximum at $\psi_0 = \psi^*$ is $(n+1)^2$ (=4.07) times the value at $\psi_0 = 0°$. The result (4.10) might be visualized as follows: For $0° \le \psi_0 \le \psi^*$ light is refracted at a virtual plane water-ice interface and the refracted wave is scattered by inhomogeneities on the ice side. For $\psi_0 > \psi^*$ it is the evanescent wave that is scattered by the same inhomogeneities. The penetration depth of the evanescent wave at a water-ice interface is always larger than 70 nm.

In Fig. 5, the light scattering cross section (4.10) is compared with the measured intensity. In the measured range $55° \le \psi_0 \le \psi^*$ the agreement is surprisingly good; however, for $\psi_0 > \psi^*$ the measured intensity is much higher than calculated. As a second discrepancy between theory and experiment we note that the factor $\cos\psi$ in (4.10) is zero for $\psi = 90°$ so that the intensity scattered parallel to the interface should vanish. This is not observed. One has to conclude that the model of the rough interface does not

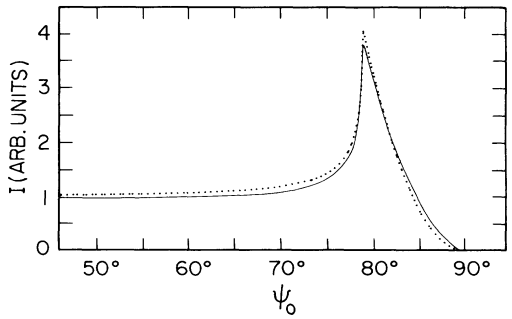

FIG. 15. Calculated scattered intensity as a function of the angle of incidence expected for a rough interface (solid line) compared with the square of the electric field amplitude at the ice side of a flat interface (dotted line).

explain the experimental results over the whole range of ψ_0 and ψ.

In order to explain the failure of this mode we consider two possibilities.

(1) The approximations underlying the calculations are not applicable because the amplitudes ζ of the surface roughness are not small compared to the wavelength of light.

(2) The model is wrong. The light is not scattered by a sharp, rough interface. In the interpretations of the linewidth measurements in Sec. IV C we will show that this is really the case.

B. Light scattering from an interface layer

In this section we calculate the angular dependence of the intensity of the light scattered by a turbid interface layer with an effective index of refraction n_1 with a value between n_i and n_w. The result will be compared to the scattering of a sharp rough interface.

The layer model is depicted in Fig. 16. The following simplifying assumptions are made.

(1) A layer exists between water and ice.

(2) The water-layer and layer-ice interfaces are sharp and smooth.

(3) The thickness d of the layer is large compared to the wavelength of light.

(4) The light is scattered within the layer by entropy fluctuations.

(5) The scattering intensities arising from the different parts of the zigzag path of the primary beam inside the layer are additive.

For a fixed direction of observation the scattered intensity is then given by

$$I(\psi_0) \propto \sum_{j=1}^{\infty} |E_j|^2 . \tag{4.12}$$

The electric field amplitudes E_j can be calculated by the recursion formulas

$$\begin{aligned} E_1 &= tE_0 , \\ E_{2k} &= r_i E_{2k-1} , \\ E_{2k+1} &= r_w E_{2k} , \end{aligned} \tag{4.13}$$

where $k=1,2,3,\ldots$, and where t is the transmission coefficient water-layer and r_i and r_w the reflection coefficients layer-ice and layer-water, respectively.

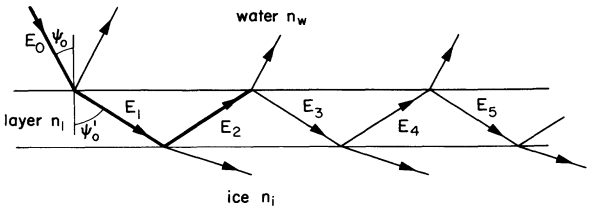

FIG. 16. Model of the interface layer. ψ_0, angle of incidence; ψ_0', angle of refraction water-layer; E_i, electric field amplitudes; n_x $(x=w,l,i)$; refractive indices of water, layer and ice.

In our experiments the field amplitude E_0 of the incident beam is parallel to the plane of incidence. The Fresnel formulas then yield

$$t = \frac{2n_1 n_w \cos\psi_0}{n_1^2\cos\psi_0 + n_w(n_1^2 - n_w^2\sin^2\psi_0)^{1/2}} , \tag{4.14}$$

$$r_x = \frac{n_x^2\cos\psi_0' - n_1(n_x^2 - n_1^2\sin^2\psi_0')^{1/2}}{n_x^2\cos\psi_0' + n_1(n_x^2 - n_1^2\sin^2\psi_0')^{1/2}} , \quad x=i,w . \tag{4.15}$$

By inserting (4.13) in (4.12) one obtains for the scattered intensity

$$I(\psi_0) \propto \begin{cases} t^2 \dfrac{1+|r_i|^2}{1-|r_i|^2|r_w|^2}, & \psi_0 < \psi_1^* \\ |t|^2, & \psi_1^* \le \psi_0 \le 90° \end{cases} \tag{4.16}$$

where $\psi_1^* = \arcsin(n_1/n_w)$ is the angle of total reflection at the water-layer interface. The function $I(\psi_0)$ is plotted in Fig. 17 for indices of refraction of the layer $n_i \le n_1 \le n_w + 0.1$.

The intensity I increases by less than a factor of 2 at the angle of total reflection if $n_1 > n_w$. If the layer had the same index of refraction as water the intensity would increase by a factor of 2 (case of ice cluster model). Such an increase was actually observed in the intensity of the Brillouin lines: If the primary beam is totally reflected at the water-ice interface the intensity of the Brillouin lines is doubled as compared to bulk water.

In the range $n_i < n_1 < n_w$ the calculated intensity increase is more than a factor of 2. There is always a sharp maximum between ψ^* and 90°. It diverges (Born's first approximation does not conserve energy) at the angle of total reflection ψ_1^* because $r_w r_i = 1$ in (4.16).

For $\psi_0 > \psi_1^*$ the square of the amplitude of the evanescent wave at the water-layer interface is plotted in Fig. 17. According to assumption (3) the effective volume in which the evanescent wave is scattered is negligible compared to the volume of the layer.

For $n_1 = n_i$ the light is refracted at an ice-water interface. This case was already discussed in Sec. IV A. If we suppose that the second maximum of the scattered intensi-

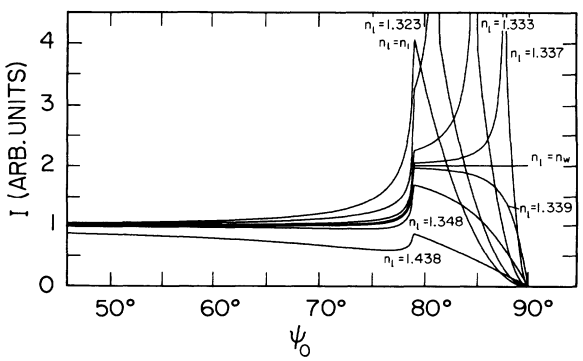

FIG. 17. Intensity of the scattered light vs the angle of incidence calculated according to the interface layer model for different refractive indices n_1.

ty, observed always at about $\psi_0=85°$, is due to an interface layer of the type discussed above, its refractive index would have to be $n_1=1.333$. Using this value, and assuming that the interface layer is waterlike one can calculate its density by means of an empirical relation based on the Lorentz-Lorenz formula. According to Eisenberg[25] the dependence of the refractive index n of water on the density ρ (in g cm^{-3}) and the temperature T (in °C) can be approximated by

$$n=1+A\rho^B e^{-CT} . \tag{4.17}$$

For $\lambda=488$ nm the constants A, B, and C are $A=0.338\,06$, $B=0.971\,88$, and $C=-7.0984\times10^{-5}$. In particular, one has for $T=0$ °C

$$n=1+0.338\,06\rho^{0.971\,88} . \tag{4.18}$$

Some refractive indices computed according to (4.18) are listed in Table II. The density that corresponds to the empirical value $n_1=1.333$ is $\rho_1=0.985$ g cm^{-3}. To illustrate this value we note that water at -8.5 °C (and at atmospheric pressure) has the same density [the dependence of n on temperature is negligible according to Eq. (4.17) for $-8.5\leq T\leq0$ °C]. Moreover, if one inserts the density of ice at 0 °C (and at atmospheric pressure) into the expression (4.18) one obtains $n=1.3107$, which is rather close to n_i. Near $\psi_0=90°$ the scattered intensity is larger than that predicted by the layer model.

In order to account for the discrepancies between the model and the measurements one has to consider refined models.

(a) Instead of the two discontinuous changes of the refractive index at the two layer boundaries there might be a continuous change.

(b) The thickness of the layer might be comparable to the wavelength of the light, so that the theory of dielectric waveguides should be applied.

In view of the limited reproducibility of our intensity measurements we abstain from a calculation of refined models, because these would necessarily involve more adjustable parameters.

C. Evidence for an interface layer from linewidth measurements

In the case of coherent elastic or quasielastic scattering in a three-dimensional medium choosing the scattering vector k means to single out the scattering due to the spatial Fourier component k of the scattering density. The length of k is given by

$$k=(4\pi n/\lambda)\sin(\theta/2) , \tag{4.19}$$

where θ is the scattering angle, λ the wavelength of light, and n the effective index of refraction of the medium.

In contrast to the above situation the Fourier decomposition of a rough surface contains only terms with wave vectors parallel to the interface. Grating theory implies that the projection of the scattering vector k onto the interface is equal to the wave vector p of the observed interface fluctuation. p is given by

$$p=(2\pi n/\lambda)(\sin^2\psi_0+\sin^2\psi-2\sin\psi_0\sin\psi\cos\Theta)^{1/2} . \tag{4.20}$$

In the special case $\psi_0=\psi=90°$ (4.20) reduces to (4.19) with $\Theta=\theta$. The scattering vector is then parallel to the interface, and p is equal to k.

The model of the fluctuating interface proposed by Güttinger *et al.*[10] predicts that the linewidth Γ should be proportional to the square of the projection of the scattering vector onto the interface, p^2, and not to the square of the scattering vector, k^2. The experimental data represented in Fig. 6 show, however, that Γ is proportional to k^2, where D_i designates a diffusion constant

$$\Gamma=D_i k^2 . \tag{4.21}$$

This observation is compatible only with three-dimensional fluctuations with isotropic dynamics. Thus the interface region cannot be sharp. It must have a finite thickness. The model of the rough interface is ruled out once more.

D. Thickness of the interface layer

The direct measurement of the thickness of the interface layer d by means of a microscope is impossible in our zone refining apparatus because of the large distances involved. An indirect method could be based on the fact that a continuous interface produces for linearly polarized light incident near the Brewster angle a small ellipticity of the reflected light, which is related to the thickness of the layer.[26] Unfortunately the zone melting apparatus does not permit measurements near the Brewster angle.

An entirely different method to obtain information on the thickness of the layer is based on the measurement of the width Γ of the Rayleigh line at small scattering angles. We have observed that Γ does not depend upon the direction of the scattering vector but only on its length, and this for scattering angles as low as at least 15°. This corresponds to a wavelength of the Fourier components as large as 1.4 μm. This length can be interpreted as a lower limit for the thickness d of the layer with the argument that the dynamics of the Fourier components in the layer can be only isotropic if their wavelengths are small compared to d.

The simultaneous variation of the linewidth described in Sec. III A 2 (see also Fig. 8) demonstrates again the iso-

TABLE II. Refractive indices of water as calculated by Eq. (4.18) for different hypothetical densities.

ρ (g cm^{-3})	$\rho_w=0.9998$	0.9900	0.9850	0.9800	0.9500	0.9250	$\rho_i=0.916\,71$
n	$n_w=1.3380$	1.3348	1.3331	1.3315	1.3216	$n_i=1.3135$	1.3107

tropic behavior of the interface layer for fluctuation wavelengths of at least 1.2 μm (scattering angle of 17.5°). The variations of Γ with time are caused by a corresponding variation of the diffusion constant in the layer.

E. Intensity of the scattered light

In the classical theory of light scattering the intensity of the light is proportional to the mean-square fluctuations of the optical dielectric constant $\langle(\Delta\epsilon)^2\rangle$ about its mean value in the scattering medium. Einstein[27] and von Smoluchowski[28] calculated this mean-square fluctuation as a function of the statistically independent variables ρ and T. According to Benedek[29] one obtains for the total intensity of the scattered light

$$dI=\frac{cE_0^2}{8\pi}\left[\frac{\omega_0}{c}\right]^4\left[\left[\frac{\partial\epsilon}{\partial\rho}\right]^2\rho^2\kappa_T+\left[\frac{\partial\epsilon}{\partial T}\right]^2\frac{T}{C_V'}\right]$$

$$\times k_B TV\sin^2\phi\, d\Omega\ , \tag{4.22}$$

where c is the velocity of light, E_0 the amplitude of the incident light, ω_0 the frequency of the light, V the scattering volume, ϕ the angle between the direction of E_0 and the direction of observation, κ_T the isothermal compressibility, and C_V' the specific heat per unit volume. I is independent of the scattering vector $\vec{k}$. It is well known that the correlation length ξ of the density fluctuations as well as κ_T diverge near a critical point. The scattered intensity becomes then k dependent [the theory of Ornstein and Zernike, e.g., contains the factor $(1+k^2\xi^2)^{-1}$].

According to Landau and Placzek[30] one neglects the second term in (4.22). The ratio of the intensity of the Rayleigh line I_C to the intensity of the Brillouin lines $2I_B$ is then given by

$$r=\frac{I_C}{2I_B}=\frac{C_P-C_V}{C_V}\equiv\frac{\kappa_T-\kappa_S}{\kappa_S}\ , \tag{4.23}$$

where the constants have their usual meaning. Equation (4.23) is difficult to interpret in view of the additional central peak predicted by Mountain.[31] The Mountain peak is supposed to account for relaxation phenomena occurring in viscoelastic liquids such as polypropylene glycol[32] or CCl_4.[33] Usually it is very broad and leads to an enhanced background extending from the center to the Brillouin lines. Close to the glass transition the Mountain line sharpens and is hidden under the Rayleigh line. Simple liquids such as liquid rare gases have no Mountain line.

We discuss the intensity of the light scattered in the interface layer in the framework of Eq. (4.22). From the isotropy of the intensity for scattering vectors k parallel to the interface one can infer that $k\xi<1$. Therefore, the correlation length is smaller than $1/k_{\max}\simeq\lambda/4\pi\simeq 40$ nm.

The large intensity of the central line observed after the onset of scattering cannot be attributed to the second term in (4.22) because the temperature dependence of ϵ is small according to (4.17). Therefore, the total intensity of the scattered light is proportional to κ_T (including the Mountain line, see Ref. 34).

The total scattered intensity measured at the interface before the onset of scattering is $I_0=7000$ counts/s, after the onset the maximum intensity emerging from the interface layer is typically $I_1=200\,000$ counts/s. The knowledge of the ratio I_1/I_0 permits an estimate of the ratio of the isothermal compressibilities before and after the onset of scattering. It is reasonable to assume that the factor $(\partial\epsilon/\partial\rho)^2\rho^2$ appearing in (4.22) is not affected. However, one has to take into account that the height of the scattering volumes before and after the onset is given by the diameter of the laser beam (100 μm) and by the thickness of the layer (we assume a value between the upper and the lower limit, $d=4$ μm). Then one has approximately for the scattering geometry described in III D

$$\frac{\kappa_{Tl}}{\kappa_T}\simeq\frac{200\,000}{4}\frac{100}{7000}\simeq 700 \tag{4.24}$$

and with (4.23)

$$\frac{C_{pl}}{C_p}\simeq 700\ , \tag{4.25}$$

where κ_{Tl} and C_{pl} are the isothermal compressibility and specific heat at constant pressure in the layer.

Equation (4.24) contains no assumptions about the scattering mechanism [Rayleigh, Mountain, or Brillouin, in contrast to Eq. (4.25)]. The Rayleigh-Brillouin spectra (Fig. 9) and the ratio B/A (Sec. III D) show that it is the intensity of the central line which increases at the onset of scattering and not the intensity of the Brillouin lines. Owing to the single exponential decay of the autocorrelation function of the scattered light the central line can be interpreted either as Rayleigh or as Mountain line. Conde *et al.*[35] concluded from their sound velocity measurements in water that the effect of structural relaxation cannot be seen above -20°C. Thus we assume that the central line is the Rayleigh line. By means of the Landau-Placzek ratio one can then estimate the adiabatic compressibility of the interface layer. It turns out to be the order of the adiabatic compressibility of water at 0°C.

F. Linewidth of the scattered light

The calculation of the linewidth for the model of a sharp fluctuating interface agrees surprisingly well with the measured Rayleigh linewidth as long as the scattering vector k is parallel to the interface. However, the independence of the linewidth on the direction of k is compatible only with an interface layer of finite thickness. The Brillouin scattering experiments (Sec. III B 2) and observation (4) in Sec. III A 2 demonstrate that the interface layer has properties which are more waterlike than icelike. Under the assumption that the waterlike layer may be interpreted as a simple fluid the width of the Rayleigh line is determined by the lifetime of the entropy fluctuations, which in turn are governed by thermal diffusion (for a review see Ref. 36). From the measured linewidths one obtains by means of Eq. (4.21) for the diffusion constant values in the range $1.4\times10^{-8}<D_i<5.7\times10^{-8}$ cm^2/s. The thermal diffusion within the layer is slowed down by a factor of about 10^5 compared to bulk water at 0°C

(1.33×10^{-3} cm^2/s) if the above assumption is correct.

According to mode-mode coupling schemes[37] the singular part of the thermal diffusivity in critical phenomena is related to the coherence length ξ by a Stokes-Einstein relation of the form

$$D=\frac{k_BT}{6\pi\eta\xi},\quad k\xi\ll1\ . \tag{4.26}$$

Assuming that the relation can be applied to the diffusion constant measured in the interface layer and that the viscosity is the same as for water 0 °C one obtains a coherence length in the range $20<\xi<80$ nm. In the mode-mode coupling schemes heat diffusion can be thought of as occurring by the spatial diffusion of regions of size ξ, i.e., heat transport can be interpreted as "structure transport." This view bears close resemblance to the mechanism of crystal growth, which is governed by the transport of latent heat and structure. The enhanced light scattering seems to be a manifestation of these processes. An interpretation of the linewidth measurements in terms of crystal growth has been given by Bilgram.[38]

G. Dependence of the linewidth on the intensity

During the onset of light scattering the dependence of the linewidth on the intensity can be described by the power law (3.6). With increasing intensity the linewidth decreases. A similar behavior is generally observed in light scattering studies of critical phenomena.

We discuss a possible analogy with the problem of condensation. The interface of a liquid is diffuse near the critical point and disappears there. The theory of Cahn and Hilliard[3] yields the density profile of the interface. This work was extended by Widom[4] and Fisk and Widom[5] who compared their results with experiment.

The solid-liquid interface layer ice-water exists only under nonequilibrium conditions in contrast to the gas-liquid interface. Nevertheless, it is interesting to compare the exponent α in Eq. (3.6) with the exponent expected for the diffuse gas-liquid interface near the critical point.

The following assumptions are made for both interface layers.

(1) The isothermal compressibility κ_T is uniform within a layer of thickness d, therefore the scattered intensity is given by

$$I\propto\kappa_Td\ . \tag{4.27}$$

(2) The linewidth measured at the interface layer is the critical part of the linewidth as given by the Stokes-Einstein relation. For fixed k^2 we write

$$\Gamma\propto\frac{1}{\eta\xi}\ . \tag{4.28}$$

Near the gas-liquid critical point d, κ_T, η, and ξ exhibit critical behavior. According to theory[5] the critical exponent for κ_T in the diffuse liquid-gas layer should be $\gamma\simeq1.3$, and the exponent for ξ should be $\nu\simeq\gamma/2$. Scaling arguments predict that the exponent for the thickness d should be the same as for ξ. The measurements of Meunier and Langevin[6] on SF_6 and cyclohexane-methanol show that this prediction is true. The critical exponent for the viscosity is of the order of 0.04 (Refs. 39 and 40) and is neglected. By inserting this exponent in (4.27) and (4.28) one obtains

$$I\propto\epsilon^{-\nu-\gamma}\simeq\epsilon^{-3\nu}\ , \tag{4.29}$$

$$\Gamma\propto\epsilon^{\nu}\ , \tag{4.30}$$

where $\epsilon=(T-T_c)/T_c$. Therefore, the resulting linewidth is proportional to

$$\Gamma\propto I^{-1/3}\ . \tag{4.31}$$

A direct experimental verification of (4.31) for the gas-liquid interface is not available. However, it is surprising that the measured exponent $\alpha=0.25$ at the ice-water interface is rather close to $\frac{1}{3}$. Nevertheless, we hesitate to speculate that we observe a kind of second-order transition at the ice-water interface.

V. CONCLUSIONS

If the growth velocity of an ice crystal exceeds a critical value (dependent on the temperature distribution at the solid-liquid interface) the onset of light scattering is observed at an interface layer. The thickness of this layer is between 1.4 and 6 μm. Its density is between that of water and ice, closer to that of water. The isothermal compressibility is about 700 times that of water and the

TABLE III. Some physical constants of water at 0 °C.

Density	$\rho_w=999.84$ kg m^{-3}	Ref. 41
Specific heat	$C_{pw}=4.2177\times10^3$ J kg^{-1}K^{-1}	Ref. 42
Thermal conductivity	$k_w=0.561$ W m^{-1}K^{-1}	Ref. 42
Thermal diffusivity	$\alpha_w=k_w/\rho_wC_{pw}$ $=1.33\times10^{-7}$ m^{2}s^{-1}	
Index of refraction ($\lambda=488$ nm)	$n_w=1.338\,016$	Ref. 43
Dynamical viscosity	$\eta_w=1.798\times10^{-3}$ N s m^{-2}	Ref. 42
Kinematic viscosity	$\nu_w=\eta_w/\rho_w$ $=1.798\times10^{-6}$ m^{2}s^{-1}	
Isothermal compressibility	$\kappa_{Tw}=5.0869\times10^{-10}$ m^{2}N^{-1}	Ref. 46
Adiabatic compressibility	$\kappa_{Sw}=5.0831\times10^{-10}$ m^{2}N^{-1}	Ref. 46

TABLE IV. Some physical constants of ice at 0 °C.

Density	$\rho_i = 916.71$ kg m^{-3}	Ref. 41
Specific heat (-2.2 °C)	$C_{pi} = 2.101 \times 10^3$ J kg^{-1} K^{-1}	Ref. 42
Thermal conductivity	$k_i = 2.2$ W m^{-1} K^{-1}	Ref. 44
Thermal diffusivity	$\alpha_i \simeq k_i / \rho_w C_{pi}$ $= 1.14 \times 10^{-6}$ m^2 s^{-1}	
Index of refraction ($\lambda = 491.6$ nm, -3.8 °C)	$n_i = 1.3135$	Ref. 45
Adiabatic compressibility	$\kappa_{Si} = 1.2 \times 10^{-10}$ m^2 N^{-1}	Ref. 47
Melting temperature	$T_m = 273.15$ K	Ref. 41

adiabatic compressibility is indistinguishable from that of water.

The diffusion constant in the layer, $D_i = \Gamma / k^2$, is smaller by a factor of about 10^5 than the thermal diffusion constant of water. We interpret D_i as an effective thermal diffusion constant that descibes the transport of heat involving fluctuations of order and disorder in the layer (Frenkel's "structure diffusion"). The relation between linewidth and intensity of the scattered light is similar to that observed in the case of the gas-liquid interface near the critical point.

ACKNOWLEDGMENTS

The authors acknowledge the collaboration of K. Baumann and U. Dürig during the experiments. We thank C. Jaccard for a critical reading of the manuscript. This work was supported by the Swiss National Science Foundation.

APPENDIX

Some physical constants of water and ice at 0 °C are presented in Tables III and IV, respectively.

*Present address: Brookhaven National Laboratory, Upton, NY 11973.

[1]W. K. Burton, N. Cabrera, and C. Frank, Philos. Trans. R. Soc. London, Ser. A 243, 299 (1951).

[2]J. E. Hilliard and J. W. Cahn, Acta Metall. 6, 772 (1958).

[3]J. W. Cahn and J. E. Hilliard, J. Chem. Phys. 28, 258 (1958).

[4]B. Widom, J. Chem. Phys. 43, 3892 (1965).

[5]S. Fisk and B. Widom, J. Chem. Phys. 50, 3219 (1969).

[6]J. Meunier and D. Langevin, J. Phys. Lett. (Paris) 43, L185 (1982).

[7]L. D. Landau and E. M. Lifshitz, *Statistical Physics* (Pergamon, London, 1958), p. 260.

[8]A. Voronel, I. Paperno, S. Rabinovich, and E. Lapina, Phys. Rev. Lett. 50, 247 (1983).

[9]Y. Saito and H. Müller-Krumbhaar, J. Chem. Phys. 74, 721 (1981).

[10]H. Güttinger, J. H. Bilgram, and W. Känzig, J. Phys. Chem. Solids 40, 55 (1979).

[11]R. A. Brown, J. Keizer, U. Steiger, and Y. Yeh, J. Phys. Chem. (in press).

[12]U. Dürig and J. H. Bilgram, in *Nonlinear Phenomena at Phase Transitions and Instabilities,* edited by T. Riste (Plenum, New York, 1982), p. 371.

[13]B. Zysset, P. Böni, and J. H. Bilgram, Helv. Phys. Acta 54, 265 (1981).

[14]H. R. Haller, J. Phys. E 14, 1137 (1981).

[15]H. Güttinger, M. Gautschi, and E. Serrallach, J. Phys. E 9, 936 (1976).

[16]J. Teixeira and J. Leblond, J. Phys. Lett. (Paris) 39, L-83 (1978).

[17]P. H. Gammon, H. Kiefte, and M. J. Clouter, J. Glaciol. 25, 159 (1980).

[18]D. P. Woodruff, The Solid-Liquid Interface (Cambridge University Press, London, 1973), p. 85.

[19]Lord Rayleigh, Proc. R. Soc. London Ser. A 79, 399 (1907).

[20]A. Andronow and M. Leontowicz, Z. Phys. 38, 485 (1926).

[21]A. Marvin, F. Toigo, and V. Celli, Phys. Rev. B 11, 2777 (1975).

[22]D. S. Agarwal, Phys. Rev. B 15, 2371 (1977).

[23]R. Loudon and J. R. Sandercock, J. Phys. C 13, 2609 (1980).

[24]O. Bryngdahl, in *Progress in Optics XI,* edited by E. Wolf (North-Holland, Amsterdam, 1973), p. 168.

[25]H. Eisenberg, J. Chem. Phys. 43, 3887 (1965).

[26]J. Peternely, Can. J. Phys. 59, 1009 (1981).

[27]A. Einstein, Ann. Phys. (Leipzig) 33, 1275 (1910).

[28]M. von Smoluchowski, Ann. Phys. (Leipzig) 25, 205 (1908).

[29]G. B. Benedek, in *Brandeis University Summer Institute in Theoretical Physics 1966; Statistical Physics, Phase Transitions and Superfluidity,* edited by M. Chrétien, E. P. Gross, and S. Deser (Gordon and Breach, New York, 1968), Vol. 2, p. 41.

[30]L. Landau and G. Placzek, Z. Phys. (Sowjet) 5, 172 (1934).

[31]R. D. Mountain, J. Res. Natl. Bur. Stand. Sect. A 70 207 (1966).

[32]Y.-H. Lin and C. H. Wang, J. Chem. Phys. 70, 681 (1979).

[33]W. S. Gornall, G. I. A. Stegeman, B. P. Stoicheff, R. H. Stolen, and V. Volterra, Phys. Rev. Lett. 17, 297 (1966).

[34]M. Djabourov, C. Lévy-Mannheim, J. Leblond, and P. Papon, J. Chem. Phys. 66, 5748 (1977).

[35]O. Conde, J. Leblond, and J. Teixeira, J. Phys. (Paris) 41, 997 (1980).

[36]B. J. Berne and R. Pecora, *Dynamic Light Scattering* (Wiley, New York, 1976), p. 233.

[37]L. P. Kadanoff and J. Swift, Phys. Rev. 166, 89 (1968).

[38]J. H. Bilgram, Helv. Phys. Acta 56, 863 (1983).

[39]P. Calmettes, Phys. Rev. Lett. 39, 1151 (1977).

[40]H. C. Burstyn, J. V. Sengers, and P. Esfandiari, Phys. Rev. A

22, 282 (1980).
[41]D. Eisenberg and W. Kauzmann, *The Structure and Properties of Water* (Oxford University Press, London, 1969).
[42]*Handbook of Chemistry and Physics*, 57th ed., edited by R. C. Weast (Chemical Rubber, Cleveland 1976/77).
[43]L. W. Tilton and J. K. Taylor, J. Res. Natl. Bur. Stand. 20, 419 (1938).
[44]S. C. Hardy, Philos. Mag. 35, 471 (1977).
[45]S. Koritnig, in *Optische Konstanten*, Vol. II of Landolt-Börnstein, edited by H.-K. Hellwege and A. M. Hellwege (Springer, Berlin, 1962), Pt. 8.
[46]C. L. O'Connor and J. P. Schlupf, J. Chem. Phys. 47, 31 (1967).
[47]P. V. Hobbs, *Ice Physics* (Clarendon, Oxford, 1974), p. 262.